# THE NEXT-GENERATION SOLAR CELL

## Student Author


**Dalton Chaffee** is a junior in electrical engineering and applied physics, and he began working under Dr. Bermel in the Purdue Summer Undergraduate Research Fellowship (SURF) program after his freshman year. His research interests include developing practical, sustainable energy alternatives such as solar cells to meet the needs of the world and the people who inhabit it. He has internship experience with the Oak Ridge National Laboratory and the National Institute of Standards and Technology in Boulder, Colorado. Chaffee is studying abroad at the National University of Singapore in fall 2015.


## Mentors


**Peter Bermel** is an assistant professor of electrical and computer engineering at Purdue University. His research focuses on improving the performance of photovoltaic, thermophotovoltaic, and nonlinear systems using the principles of photonics. Specific topics of interest include thin-film photovoltaic light trapping and photon recycling, as well as selective thermal emitters for high-performance thermophotovoltaics.

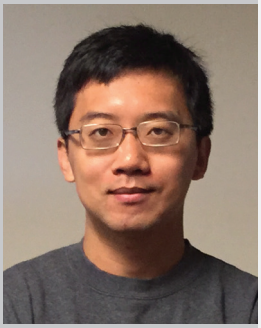

**Dr. Xufeng Wang** is a Discovery Park research associate and the technical director of the Nano-Engineered Electronic Device Simulation (NEEDS) at Purdue University. His current research focuses on the simulation, theory, and modeling of nano-electronic devices at both compact-model and detailed numerical TCAD levels.


## Abstract


Solar cell efficiencies have grown in recent years, but further improvements must be made in order for this sustainable energy technology to see widespread commercial use. Traditional solar cells use a junction near the top surface of the cell to separate charge carriers to create electric current; however, with new advances in technology and improved material quality, the role of the junction has become less clear. Recently designed high-efficiency solar cells have taken advantage of high charge carrier lifetimes to shrink the base and move the junction toward the back of the cell, away from the source of carrier generation. For example, in 2013, a GaInP solar cell was created using a rear-junction design with a base width of just 40 nanometers, yielding a record single-junction efficiency of 20.8%. The reason for this improvement, however, is not well understood. In this study, we develop a model of this record efficiency cell in a numerical device simulator to discover the mechanisms leading to the rise in efficiency. By matching simulation parameters with experimental and theoretical characteristics, we are able to show that the large electric field at the rear junction may diminish recombination due to defects in the bulk region in the cell. We also demonstrate consistent improvement in cell efficiency as the junction is moved toward the back of the GaInP cell. These results provide us with a deeper understanding of present-day high-efficiency solar cell operation and suggest how future efficiencies can be pushed closer to their theoretical limit.



Chaffee, D. (2015). The next-generation solar cell: Exploring the role of rear junctions in efficiency enhancement. *Journal of Purdue Undergraduate Research, 5,* 18–29. http://dx.doi.org/10.5703/jpur.05.1.03

## Keywords

photovoltaic cells, solar energy, heterojunctions, gallium indium phosphide, simulation, energy efficiency, recombination, thin-film devices





http://dx.doi.org/10.5703/jpur.05.1.03

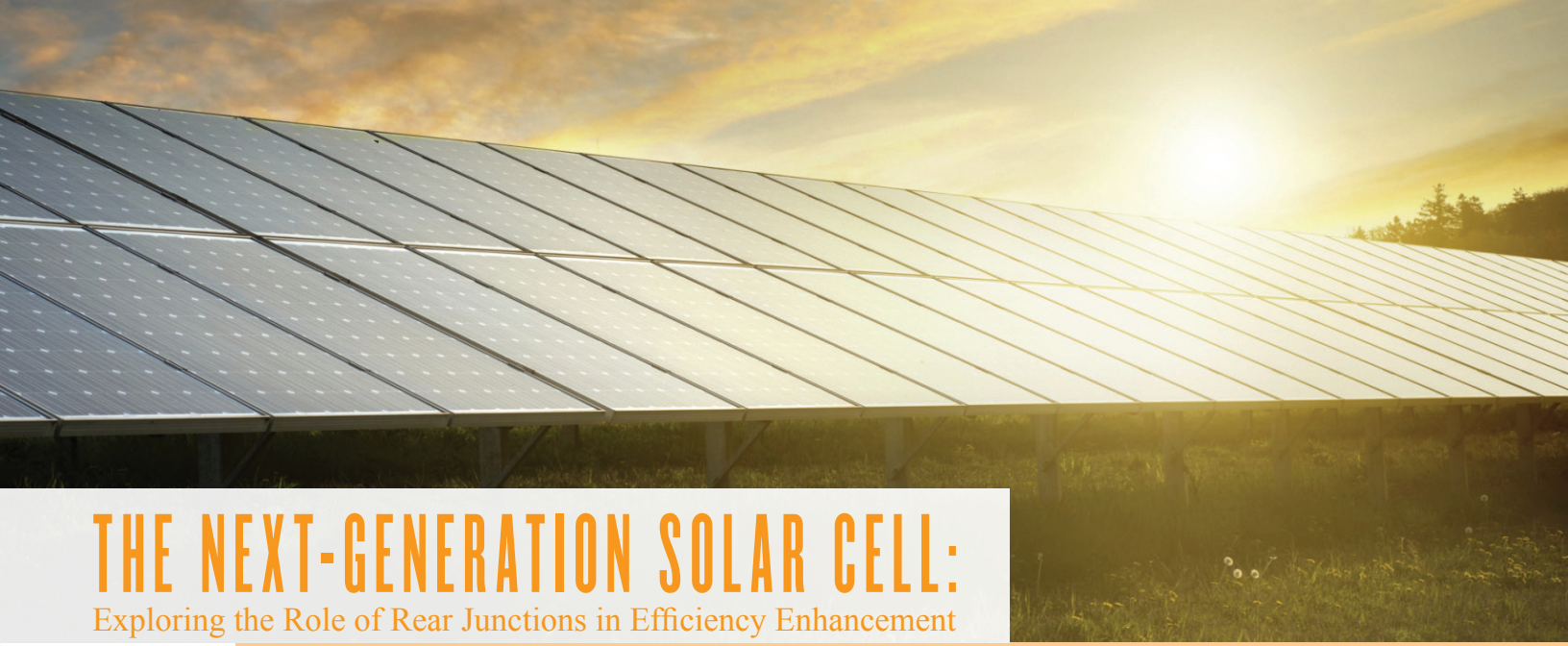

# THE NEXT-GENERATION SOLAR CELL:

## Exploring the Role of Rear Junctions in Efficiency Enhancement

Dalton Chaffee, Engineering

### INTRODUCTION

Today, much of the world's energy comes from sources that are both nonrenewable and environmentally unsustainable. Solar power has the potential to solve both of these problems, but while solar cell efficiencies have been increasing, they are still not high enough to make solar energy cost-effective without subsidies. The search for technologies that provide cheaper and more efficient solar cells is therefore crucial to the energy future of the planet. Researchers working to solve this problem have started developing a new type of solar cell that shows promise: the thin-film solar cell, which is built at a thickness (~3-40 um) of only a few percent of traditional solar cells (>200 um). Not only do these thin-film cells require less materials usage, a promising sign for their long-term economic benefits, but they also have been demonstrated to be more efficient than traditional solar cells (Figure 1). In particular, Alta Devices's thin-film gallium arsenide cell demonstrated an efficiency of 28.8% in 2012, a world record for single-junction solar cells of any thickness under standard conditions (Green, Emery, Hishikawa, Warta, & Dunlop, 2015). Despite these promising numbers, this efficiency could be pushed even higher (Shockley & Queisser, 1961) to about 33%. Thus, significant room for improvement still exists.

While solar cells have become thinner and thinner, other technological steps have been made in the push to increase solar cell efficiency. These steps have included tweaking the design traditionally considered essential to operation of the solar cell. Fundamentally, a solar cell absorbs the energy of solar photons to create electron-hole pairs and extracts these carriers with a diode in the form of electricity (Figure 2). Traditionally, the diode has been located as close as possible to the front of the cell to maximize collection of carriers, most of which are generated near the surface of the cell. However, with recent improvements in material quality that increase carrier diffusion length, researchers have experimented with moving the junction closer to the back of the cell to reduce recombination losses and to improve photon recycling, a process in which recombined photons are reflected off of the back mirror and then reabsorbed into the cell. The record efficiency thin-film GaAs solar cell built by Alta Devices deployed this strategy to obtain high efficiency (Kayes et al., 2011).

One recently developed cell that utilizes a thin-film and rear-junction design to obtain world-record efficiency is the gallium indium phosphide (GaInP) cell created by Geisz, Steiner, Garcia, Kurtz, and Friedman (2013). Though GaInP is not as ideal for single-junction cells as gallium arsenide or silicon, it is very useful in multijunction cells (Kurtz, Myers, & Olson, 1997), making the 20.8% efficiency obtained by this single-junction GaInP cell important. While this thin-film, rear-junction design reached record efficiency, the exact mechanisms that occurred within the cell that led to the efficiency increase are not fully understood. The researchers who developed the cell have several theories as to why the rear-junction cell performed better, including lower Sah-Noyce-Shockley (SNS) recombination at the junction and better photon recycling, but because certain parameters are difficult or impossible to obtain experimentally, their hypotheses could not be verified.

Theoretical modeling of solar cells is a method that has been used for decades to identify areas of improvement for current designs (e.g., Lush & Lundstrom, 1991). The advantages of theoretical modeling are numerous: it

allows for frequent, quick, and inexpensive trials; exploration of parameter space that may otherwise be impossible given current experimental methods; and precise tracking of any numerical parameter within the simulation. In this work, we use Sentaurus, a commercial semiconductor device software simulator, in order to comprehensively model the thin-film GaInP solar cell (Figure 3). We tracked the behavior of the cell as the model was altered from the traditional, front-junction design to the new, rear-junction design. We found that while the rear-junction design does in fact exemplify lower overall SRH recombination, it is in the bulk region rather than the depletion region that the greatest advantage is seen. We also verify the trend that narrowing the base region of the thin-film solar cell design does indeed lead to higher overall efficiencies. These results will pave the way for further innovation in solar cell design as researchers push the limits of this technology in order to provide the world with a clean, renewable, affordable energy source.

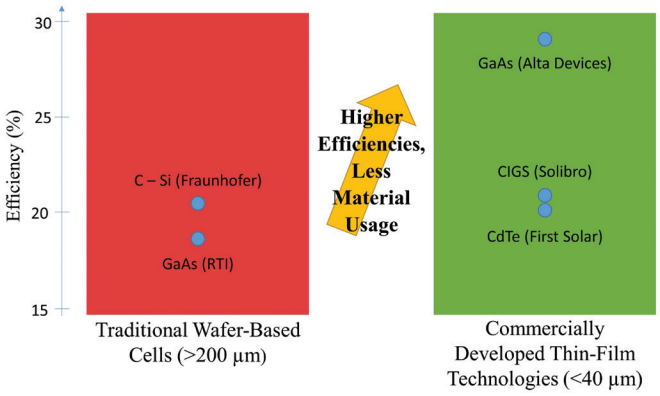


**Figure 1.** A demonstration of the increased efficiencies seen by recently developed thin-film solar cells.

## SOLAR CELL BASICS

The purpose of a solar cell is to absorb the energy of the solar photons that strike the surface of the cell by using special properties of semiconductors. In order for this to occur, several things must be true:

1. The photons must pass into the cell rather than reflecting off the top surface, and they must stay inside the cell until they are absorbed.

2. The photons must have enough energy to create an electron-hole pair in the semiconductor lattice.

3. The electron-hole pairs must then be separated and collected as current before they lose their energy and recombine.

4. A voltage must be applied across the load in order to collect power.

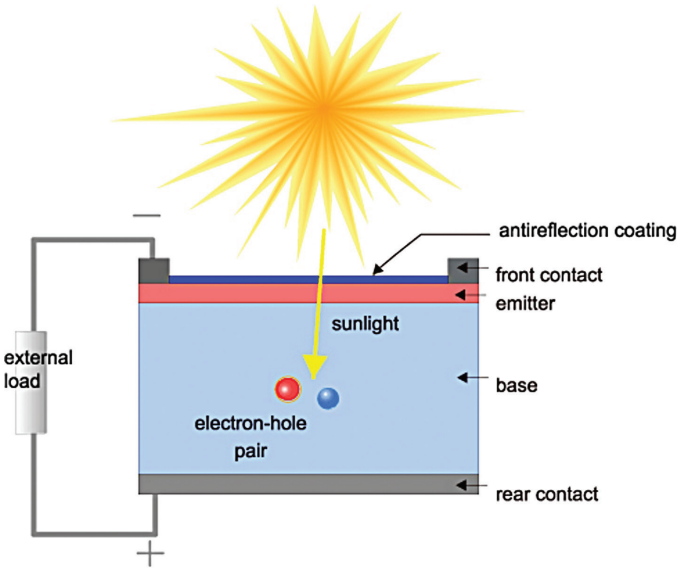


**Figure 2.** The configuration of a basic solar cell (Bowden & Honsberg, 2014).

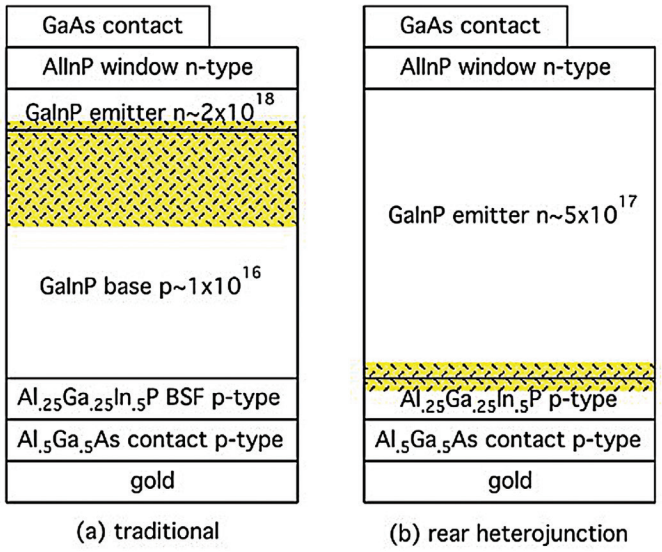


**Figure 3.** GaInP structures developed by Geisz et al. (2013). The structure in (b) demonstrated world-record efficiency. Yellow shading indicates approximate depletion region.

The first item on this list depends mostly on optical considerations. One or more optical layers of desirable refractive coefficients and thicknesses are usually placed on the top of any solar cell in order to minimize reflection off of the top surface. This is known as an anti-reflection coating (Figure 2). In addition, the back layer of some solar cells, particularly thin-film cells, have reflective back surfaces in order to reflect unabsorbed photons back through the cell for another pass.

The energy of a photon is given as:

$$E = \frac{hc}{\lambda} \tag{1}$$

where $h$ is Planck's constant, $c$ is the speed of light, and $\lambda$ is the wavelength. In order to absorb a photon, the energy of the photon must exceed the band gap of the semiconductor, $E_g$. The energy gathered from any single photon is given as:

$$E_{absorbed} = \begin{cases} E_g, E \geq E_g \\ 0, E < E_g \end{cases} \tag{2}$$

Optimizing this function for a single-junction cell under the standard sunlight spectrum requires $E_g \cong 1.1$ eV (Shockley & Queisser, 1961).

The focus of much solar cell design is the collection of carriers. In a basic solar cell, the topmost active layer in the cell, known as the *emitter,* is doped with either electrons or holes, and the layer immediately below, known as the *base,* is doped in the opposite way (Figure 2). Doping is a process in which semiconductors are injected with atoms of a certain structure such that there is either an excess amount of electrons (n-type) or a dearth of electrons (i.e., an excess amount of holes [p-type]) in the lattice. This process makes the material more conductive. In addition, when two semiconductors of opposite doping are pushed together, the result is what is known as a *p-n junction.* This junction acts as a diode, separating electrons to one side of the diode and holes to the other by means of a strong electric field. Having this junction in the semiconductor allows charge to flow, and thus current to run.

Not all electron-hole pairs that are created by incoming photons will be collected by the junction. Some will lose their energy by way of certain mechanisms known collectively as *recombination*. The first type of recombination is known as *radiative recombination,* and it is a fundamental loss in solar cells. Radiative recombination occurs when an excited electron loses its energy and falls directly down across the band gap to recombine with a hole, radiating a photon with $E \cong E_g$ in the process. The amount of radiative recombination (measured in charge per second per volume) is given by:

$$R_{rad} = B(np - n_i^2) \tag{3}$$

where $B$ is the radiative $B$-coefficient, $n$ and $p$ are the electron and hole concentrations as defined by the doping level, and $n_i$ is the intrinsic carrier concentration of the material.

Shockley-Read-Hall (SRH) recombination occurs when electrons gradually lose their energy due to defect levels in the material, rather than losing it all at once. In a perfect material, SRH recombination would not exist; however, due to defects introduced in processing, the effects of SRH recombination are not only present but often dominant in solar cells. SRH recombination also tends to be particularly prevalent around the junction of a solar cell, where it is sometimes called SNS recombination. The amount of SRH recombination is given approximately for doped semiconductors by:

$$R_{SRH} = \begin{cases} \frac{n}{\tau_{SRH}}, \text{p-type} \\ \frac{p}{\tau_{SRH}}, \text{n-type} \end{cases} \tag{4}$$

where $\tau_{SRH}$ is the SRH lifetime of the material, in seconds. This lifetime is the average amount of time a carrier will travel before recombining via SRH.

Other recombination parameters can also play a factor in solar cells. These include surface recombination, characterized by the surface recombination velocity, and Auger recombination, a process by which one excited electron transfers its energy to another excited electron. The energy is still lost here because the first electron recombines with a hole while the second electron ultimately relaxes to its initial, bandgap energy.

Because radiative recombination is the most fundamental recombination process, solar cell designs often focus on minimizing the other types of recombination. Thus, the external radiative efficiency, defined as:

$$ERE = \frac{R_{Rad}}{R_{Total}} \tag{5}$$

where $R_{Total}$ is the total recombination (including radiative), should be high in an efficient solar cell. One exception to this rule—that is, one way to decrease $R_{Rad}$—is to take advantage of a process known as photon recycling. Photon recycling occurs when a photon that has been radiatively emitted is collected once again by the cell. This effect is greatly enhanced in thin-film designs that incorporate a backside mirror, and it can result in a much-diminished $B$-coefficient.

The current collected by the solar cell when no voltage is applied at the terminals of the cell is known as the short-circuit current ($J_{sc}$). As a voltage (also known as a bias) is applied, power is generated as P = IV. However, at greater bias, recombination becomes more and more prevalent, decreasing the current (Figure 4). Eventually, all of the current is lost to recombination at a bias known as the open-circuit voltage ($V_{oc}$). At some bias in-between $J_{sc}$ and $V_{oc}$, the power is maximized. It is at this point that the efficiency of a solar cell is measured.

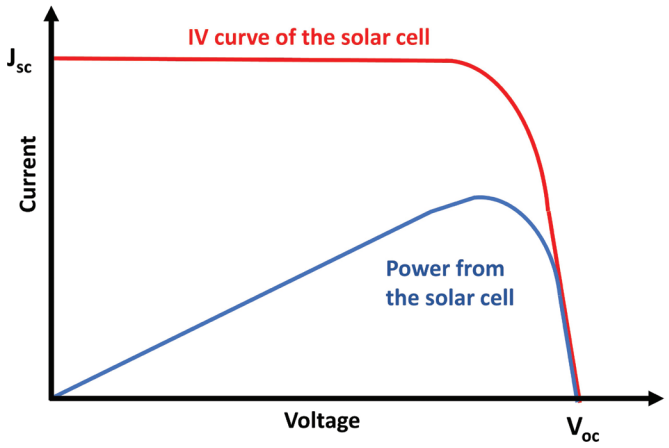


**Figure 4.** A characteristic IV curve of a solar cell. Notice that at higher applied voltages, recombination inevitably causes the current to decrease (Bowden & Honsberg, 2014).

## METHODS

Sentaurus is used in a wide variety of semiconductor applications. Because the user has control over so much of the simulation, it was considered an ideal simulator for the nontraditional solar cell structures that we model in this study. Layer thicknesses, doping, incident light, material parameters (including recombination parameters), and bias can all be easily inputted and varied. Results, including output current, recombination, band energy diagrams, and electric field, can be retrieved as a function of spatial position or as a function of voltage. A sample Sentaurus output is shown in Figure 5.

The first step in our process was to develop simulations of both the rear-junction and front-junction designs. These were done according to the material parameters outlined in Geisz et al. (2013), as shown in Figure 6. The resulting band energy diagrams outputted by Sentaurus also are included. A summary of some material parameter values used for each layer of the cell are shown in Table 1, including some that were not explicitly given in Geisz et al. (2013) but were instead estimated from the literature.

Certain recombination parameters, including the radiative *B*-coefficient, SRH lifetime, and surface recombination velocity, were not explicitly provided in this experiment, and their values can vary widely depending upon material quality, processing procedures, and sample-to-sample variation. We used both literature recombination parameters and parameters fitted to the experimental data in an effort to capture qualitative and quantitative behavior of the cell. Once these parameters were established, many different outputs, including recombination with respect to bias, spatial recombination, surface recombination, and cell performance with varying base thicknesses, were analyzed in order to pinpoint the mechanisms leading to the record efficiency.

## RESULTS

### Literature Recombination Parameters

First, recombination values from the literature were used to model the front- and rear-junction structures; these values are summarized in the first row of Table 3. The *B*-coefficient was scaled down by a factor of 100 from that reported in Ioffe Physico-Technical Institute (2001) to account for photon recycling, and the SRH lifetime was based off of other high-performance cells. Using these recombination parameters, the simulation bias was varied from $J_{sc}$ to $V_{oc}$ to examine the effect of different recombination mechanisms on each design. Figure 7 shows the resultant IV and recombination curves from these simulations. At each point, the recombination due to each mechanism was integrated throughout the entire cell; this value is displayed in units of current. These plots show which mechanism(s) dominated in each case. It can be seen that while SRH recombination was the dominant mechanism in the front-junction structure, the rear-junction structure had no single dominant mechanism, but rather comparable contributions from each mechanism. This indicates that the rear-junction structure had less SRH recombination and corresponds to the higher radiative efficiency seen in the experiment.

Next, we examined the effects of surface recombination velocity at the base/BSF interface. Table 2 shows the percentage of total recombination due to surface recombination at $V_{oc}$ for different surface recombination velocities. It can be seen that surface recombination plays a much more substantial role in the rear-junction design, particularly at intermediate surface recombination velocities.

Additionally, we looked at SRH recombination as a function of position at $V_{oc}$ (Figure 8). Here, we see the greatest

| Material Layer | Band Gap (eV) | Electron Affinity (eV) | Mobility ($cm^2/(Vs)$) (n,p) | Density of States (n,p) |
|---|---|---|---|---|
| AlInP Window | 2.3 | 3.78 | (100, 10) | ($1*10^{20}$, $1*10^{19}$) |
| GaInP Emitter, Base | 1.81 | 4.01 | (500, 30) | ($1.3*10^{20}$, $1.28*10^{19}$) |
| AlGaInP BSF/Base | 2.39 | 3.43 | (100, 50) | ($1*10^{20}$, $1*10^{19}$) |

**Table 1.** Literature values for various material parameters for electrons (n) and holes (p) for each layer in the structure (Brown et al., 2006; Geisz et al., 2013; Haas, Wilcox, Gray, & Schwartz, 2011; Zhang & Gu, 2012).

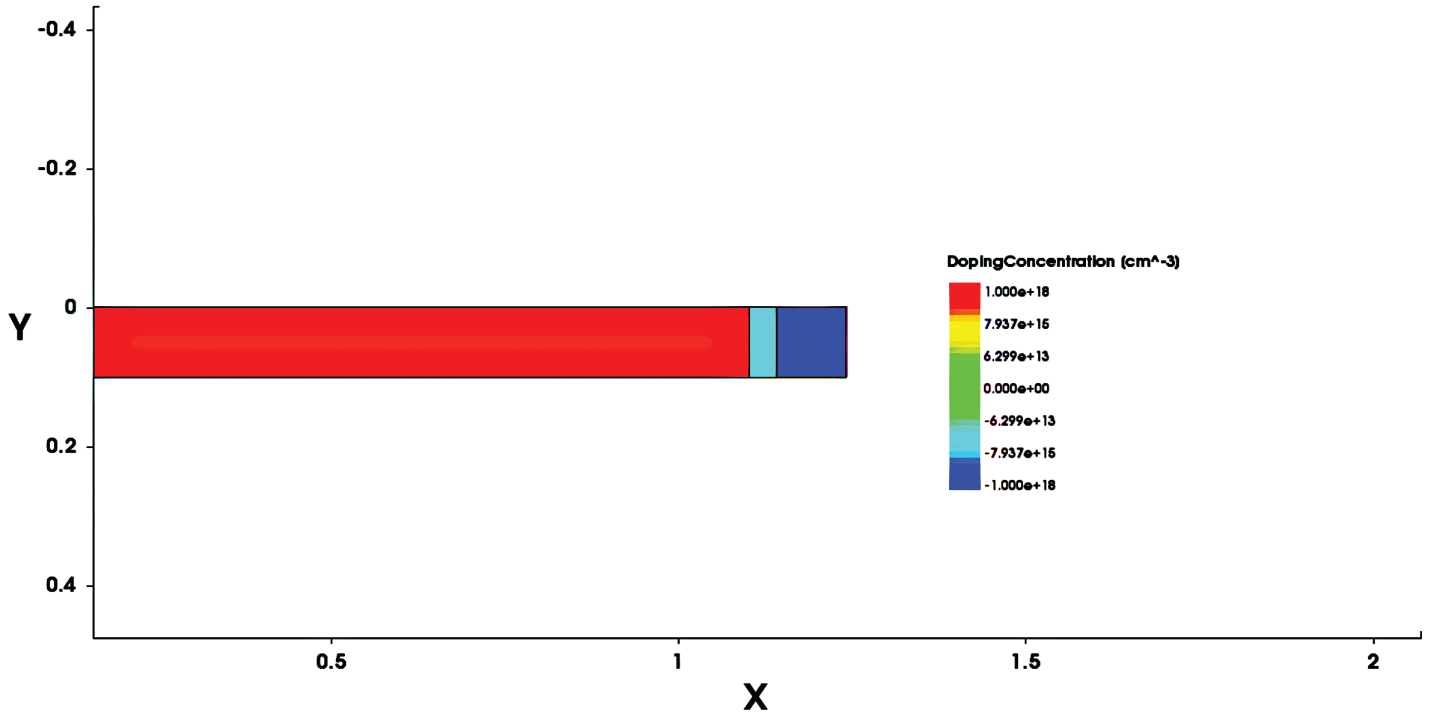


**Figure 5.** Visual representation of rear-junction structure from Sentaurus. The top of the cell corresponds to the left-hand side of the figure.

difference in the two structures. The electric field is shown to highlight the location and width of the depletion region in the two designs—the band energy diagrams (Figure 6) also evince the difference. From Figure 8, it can be seen that while the peak SRH recombination in the depletion region is greater for the rear-junction design, the amount of recombination in the rest of the structure is lower than the bulk recombination in the front-junction structure.

## Fitted Recombination Parameters

While the literature recombination values were a good estimate, they did not yield a perfect match between the simulated and experimental cell performance (Table 4). Furthermore, these values can vary widely, due not only to processing techniques, but also simply to sample-to-sample variation (Gaubas & Vanhellemont, 2007). In order to better match the simulated and experimental cell performance, the *B*-coefficient and SRH lifetime were fitted to the experimental data. The results of these simulations were analyzed similarly to those produced from literature recombination parameters.

In order to determine the fitted *B*-coefficient and SRH lifetime, we first developed the rear-junction model with only radiative recombination. The theoretical maximum open circuit voltage of the cell if only radiative recombination is present, $V_{oc}^{rad}$, can be determined by

$$V_{oc}^{rad} = V_{oc} - \frac{kT}{q} * ln(\eta_{ext}), \quad (6)$$

where $V_{oc}$ is the experimental $V_{oc}$, $k$ is Boltzmann's constant, $T$ is temperature, $q$ is the fundamental charge, and $\eta_{ext}$ is the external radiative efficiency determined by theoretical methods (Geisz et al., 2013). We varied the *B*-coefficient of the model until the simulated $V_{oc}$ matched the theoretical limit of $V_{oc}^{rad}$. Next, using this radiative *B*-coefficient, we introduced SRH recombination into the model. We varied the SRH lifetime until the simulated $V_{oc}$ matched the experimental $V_{oc}$. In implementing this method, we assumed that other types of recombination, including surface and Auger, are negligible. As before, the fitted *B*-coefficient is an effective value—it includes photon recycling effects, which were not calculated explicitly in the simulation. The fitted values gained by this method are summarized in the second row of Table 3. While these values were orders of magnitude from the literature values, they produced a much better match with the experimental results, as indicated in Table 4.

The simulations with fitted recombination parameters were analyzed similarly to the simulations that used literature values. In Figure 9, it can be seen that while SRH recombination dominated both structures, its effect was lessened in the rear-junction case. Table 5 shows that even at very low surface recombination velocities, surface recombination can play a critical role in both the front- and rear-junction designs given the fitted parameters. At surface recombination velocities of 100 cm/s and above, other recombination mechanisms become almost negligible. In Figure 10, a similar pattern can be seen as in Figure 8, although in this case the lack of bulk recombination in the rear-junction

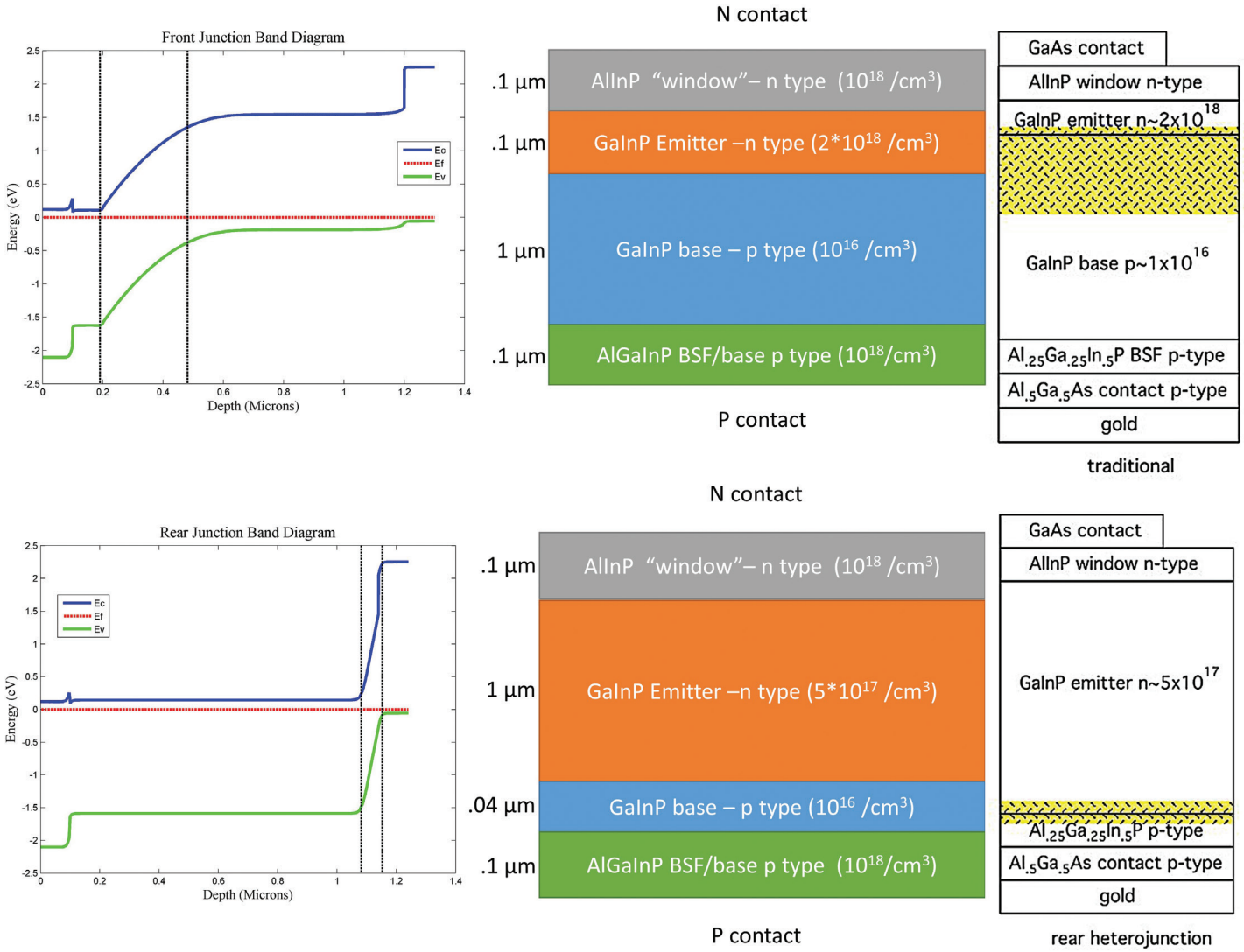


**Figure 6.** The structures inputted into Sentaurus (center). The front-junction structure is shown at top and the rear-junction structure on bottom. These were modeled after the parameters outlined in Geisz et al. (2013) (right). The window layer and gold rear-mirror were accounted for by adjusting the front and rear reflectance in the simulation. The energy band diagrams for the structures at equilibrium, as outputted by Sentaurus, are shown at left. The black dashed lines demarcate the respective depletion regions.

| Surface Recombination Velocity | Rear Junction | Front Junction |
|---|---|---|
| S = 1 cm/s | 0.5% | 0.0% |
| S = 100 cm/s | 30% | 2.5% |
| S = 10,000 cm/s | 94% | 67% |

**Table 2.** The simulated percentage of recombination due to surface recombination at the base/BSF interface at literature parameters. While the estimated recombination rate from the literature is 100 cm/s, different experimental parameters can make this number vary widely in practice.

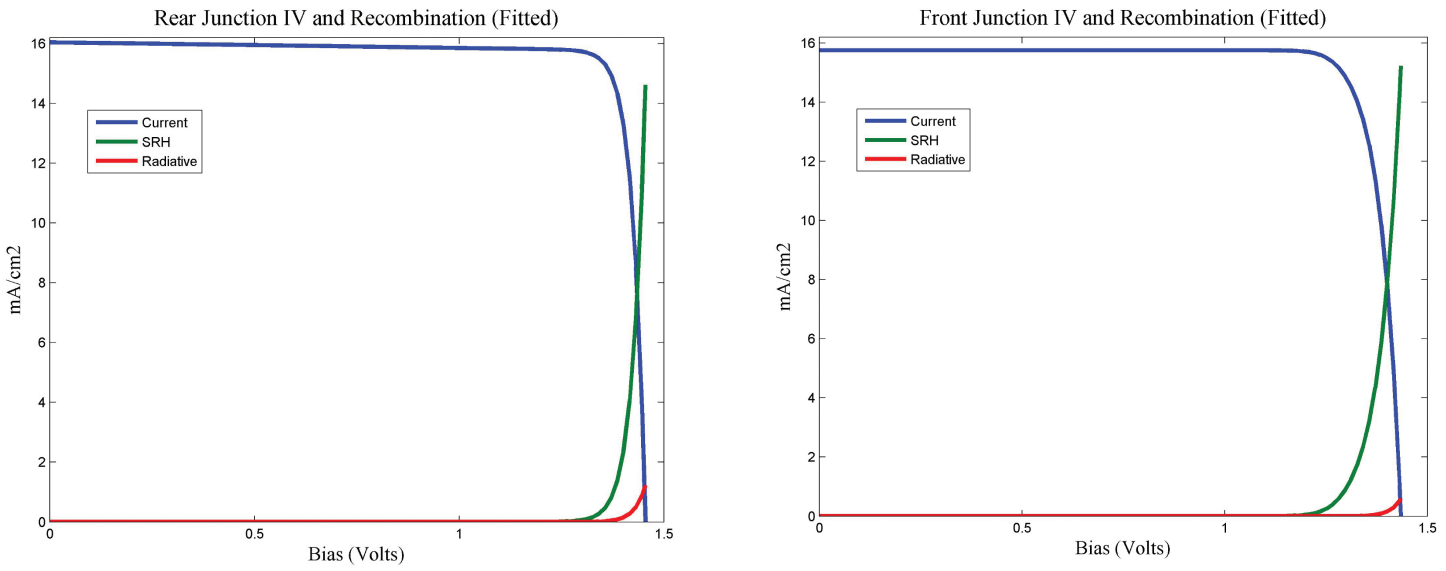


**Figure 7.** The simulated effects of various recombination mechanisms on both the front- and rear-junction designs at literature recombination values. Notice the decreased SRH recombination and relative importance of other mechanisms in the rear-junction structure.

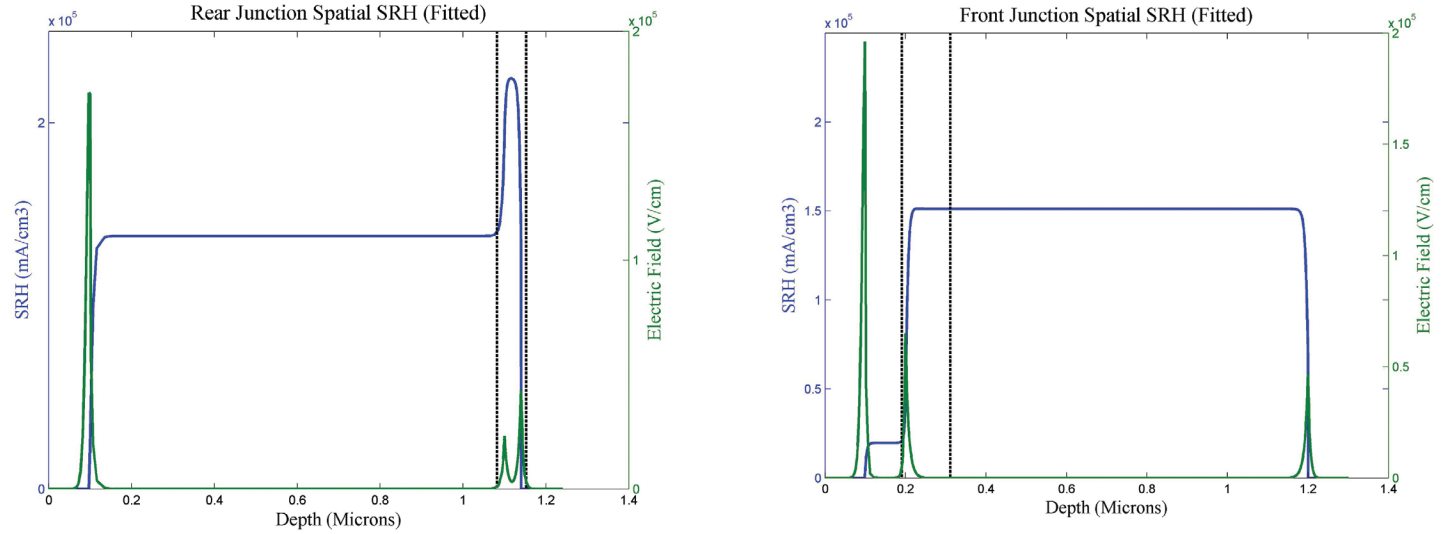


**Figure 8.** The simulated spatial SRH recombination versus position for the front- and rear-junction solar cell designs at literature recombination values. The black dashed lines indicate the borders of the depletion region in each structure, which are defined by the electric field at the junction. Notice the higher electric field throughout the depletion region of the rear junction; this contributes to carrier collection.

| | Radiative B-coefficient ($cm^3/s$) | SRH Lifetime (µs) | Surface Recombination Velocity (GaInP/AlGaInP) (cm/s) | Auger Recombination Rate ($cm^6/s$) |
|---|---|---|---|---|
| Literature | $1.0\&10^{-12}$ (Ioffe, 2001) | 1.0 (King et al., 2003) | 100 (Ioffe, 2001) | $3.0*10^{-30}$ (Ioffe, 2001) |
| Fitted | $1.93*10^{-15}$ | 70 | - | - |

**Table 3.** Comparison of literature recombination values to those fitted from experimental data (King et al., 2003). Note the *B*-coefficient in both cases is an effective value encompassing photon recycling. Simulations were run at each set of parameters in order to obtain both a qualitative and quantitative understanding of the results.

| Parameter | Reported Value (Experimental) | Simulated Value (Literature Parameters) | Error | Simulated Value (Fitted Parameters) | Error |
|---|---|---|---|---|---|
| $V_{oc}$ (Volts) | 1.455 | 1.326 | 8.9% | 1.455 | 0.0% |
| $J_{sc}$ (Volts) | 16.0 | 15.9 | 0.6% | 16.0 | 0% |
| FF (%) | 89.3 | 88.2 | 1.2% | 89.3 | 0% |
| Efficiency (%) | 20.8 | 18.6 | 10.6% | 20.8 | 0% |
| $V_{oc}$—Radiative (Volts) | 1.522 | 1.359 | 10.7% | 1.522 | 0% |
| External Radiative Efficiency (%) | 7.64 | 27.9 | 265% | 8.43 | 10.3% |

**Table 4.** Comparison of solar cell parameters of interest from the experiment, simulated using literature recombination parameters, and simulated using fitted parameters. Notice that with fitted parameters, all parameters of interest, with the exception of external radiative efficiency (ERE), matched perfectly.

| Surface Recombination Velocity | Rear Junction | Front Junction |
|---|---|---|
| S = 1 cm/s | 36% | 21% |
| S = 100 cm/s | 84% | 60% |
| S = 10,000 cm/s | 97% | 86% |

**Table 5.** The simulated percentage of recombination due to surface recombination at the base/BSF interface at fitted recombination parameters. Notice that because of the low recombination rates, it takes a relatively low surface recombination velocity for surface recombination to dominate. While the estimated recombination rate from the literature is 100 cm/s, different experimental parameters can make this number vary widely in practice.

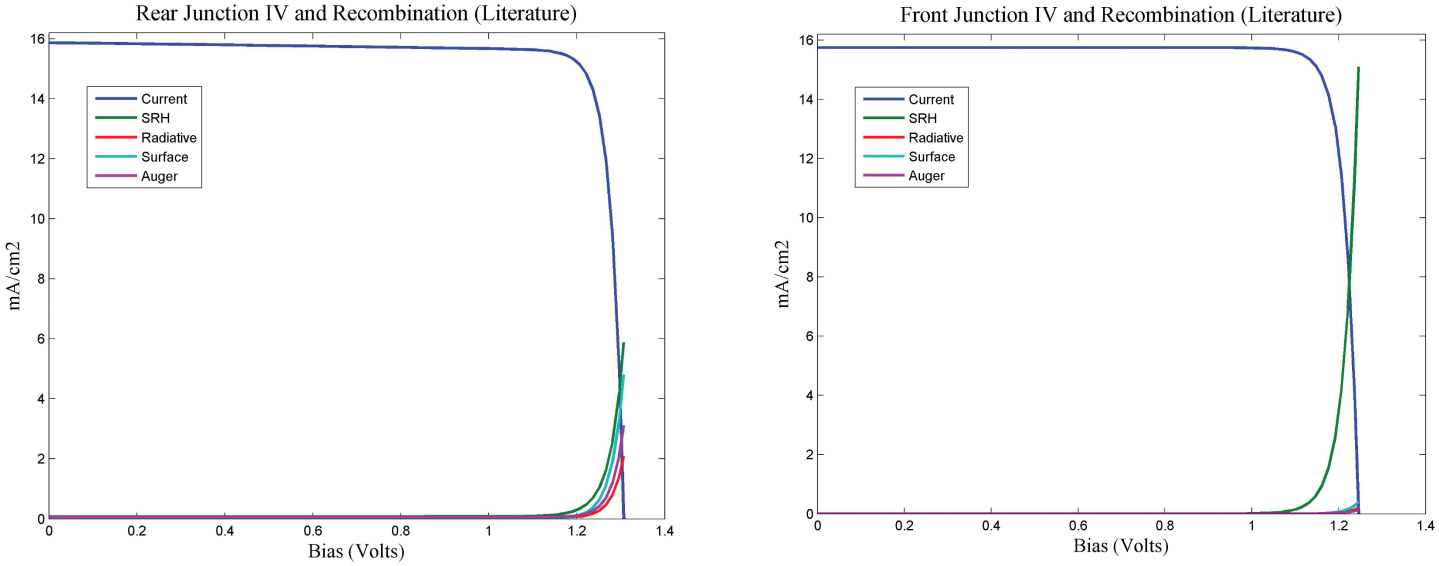


**Figure 9.** The simulated effects of various recombination mechanisms on both the front- and rear-junction designs at fitted recombination parameters. SRH recombination dominates both structures, although slightly less so for the rear-junction. Auger and surface recombination have been assumed negligible.

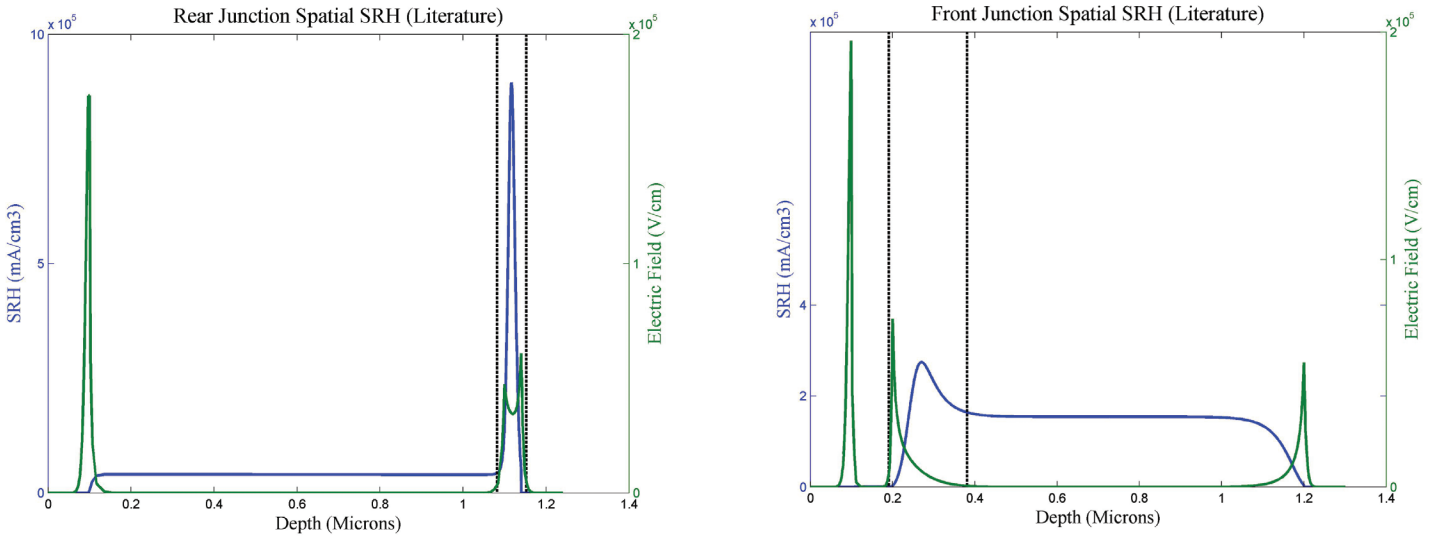


**Figure 10.** The simulated spatial SRH recombination versus position for the front- and rear-junction solar cell designs at fitted recombination parameters. The black dashed lines indicate the borders of the depletion region in each structure, which are defined by the electric field at the junction. Notice the higher electric field throughout the depletion region of the rear junction; this contributes to carrier collection.

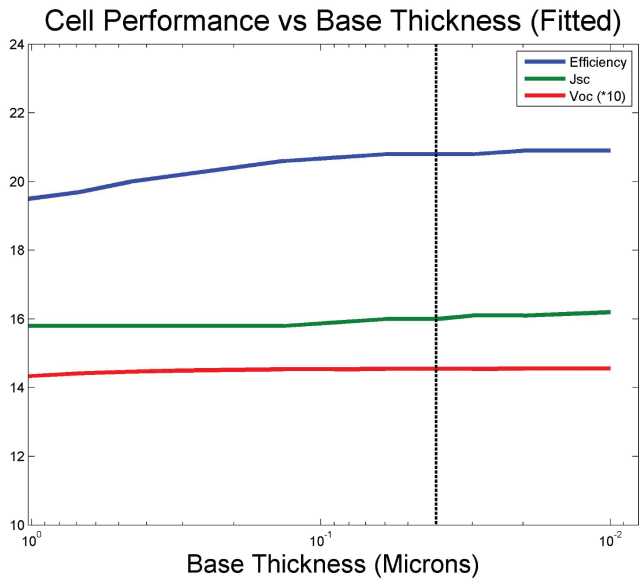


**Figure 11.** Parameters of interest for GaInP structure as the junction is moved from the front of the structure (shown on the left side of the figure) to the back side of the structure (shown on the right side of the figure) for fitted recombination parameters. The total (base + emitter) thickness of the structure was held constant at 1.04 microns. The black dashed line indicates the 40 nm base thickness that was used in Geisz et al. (2013) and for the rear-junction model in this work.

structure is not as pronounced. Finally, Figure 11 shows the effect of varying the base thickness from that of the front-junction cell (1,000 nm) to that of the rear-junction cell (40 nm) and on to a vanishingly small thickness. A steady increase in overall efficiency can be observed, although this mostly levels off around the 40 nm mark.

## DISCUSSION

We have identified several possible causes of the solar cell efficiency increase associated with shifting from the front-junction to the rear-junction structure. The first of these, suggested by Geisz et al. (2013), is improved photon recycling. The utilization of photon recycling does enable the rear-junction structure to be effective—simulations at higher radiative *B*-coefficients corresponding to no photon recycling ($B = 10^{-10}$ cm$^3$/s) degraded the efficiency of the rear-junction structure to a much greater degree. However, this appears to be solely caused by the experimenters' use of a reflective back mirror and not by the shifted junction. The fitted recombination coefficient was calculated using the rear-junction structure and $V_{oc}^{rad}$, but when the front-junction design and $V_{oc}^{rad}$ were used, an almost identical *B*-coefficient was obtained. These fitted, effective *B*-coefficients should only be dependent upon the material and photon recycling—the material is the same, so photon recycling must also be similar in order to result in the same *B*-coefficient. Thus, while utilizing photon recycling was instrumental in allowing the rear-junction design to work in the first place, it in itself was not the

cause of the rear-junction design being better than the front-junction design.

Geisz et al. (2013) also pointed out the difference in SRH recombination due to the narrow depletion region of the rear junction. The narrow depletion region is due to the high doping of the BSF layer that acts as an effective part of the p-n junction. The approximate depletion widths are 71 nm for the rear-junction structure versus 120–190 nm for the front-junction structure. Geisz et al. (2013) predicted that there would be less SNS recombination in the rear junction's narrower depletion region—however, it is in the bulk region rather than the depletion region that the rear junction really sees an advantage in SRH recombination. In Table 6, the integrated SRH recombination in both the bulk and the depletion regions is shown. The advantage of the rear-junction device is particularly noticeable under the literature parameters.

Surface recombination, while not considered by Geisz et al. (2013), may be a difference-maker between the two designs because the recombination occurs within the depletion region for the rear-junction structure, but not at all for the front-junction structure. The results did not immediately suggest that there was any difference; a glance at Figure 7 appears to show that surface recombination begins to be a factor at the same bias for each design, all else being equal. However, an interesting pattern emerges when $V_{oc}$ is plotted with respect to surface recombination velocity for each design. Figure 12 shows this pattern for both parameter sets. It can be noted that, particularly at surface recombination velocities above 100 cm/s, recombination begins to have a larger effect on the rear-junction design than on the front-junction design. On the other hand, the results in Figure 12(b) seem to indicate that the surface recombination velocity may be greater in the front-junction design. Finally, as literature estimates put the recombination at a GaInP-AlGaInP interface at 100 cm/s, it may have little impact on $V_{oc}$ in any case, if the quantitative values seen in Figure 12(a) are representative of those found in the real cell.

## CONCLUSIONS AND FUTURE WORK

The main objective of this work was to demonstrate the causes of the efficiency increase in the record-efficiency

| Surface Recombination (mA/cm²) | Front (Fitted) | Rear (Fitted) | Front (Literature) | Rear (Literature) |
|---|---|---|---|---|
| Bulk | 13.59 | 13.49 | 11.85 | 3.91 |
| Depletion | 1.64 | 1.13 | 3.24 | 1.96 |

**Table 6.** Integrated SRH recombination both within the depletion region and in the bulk region for all parameter sets. Notice that the literature bulk rear-junction recombination was very low.

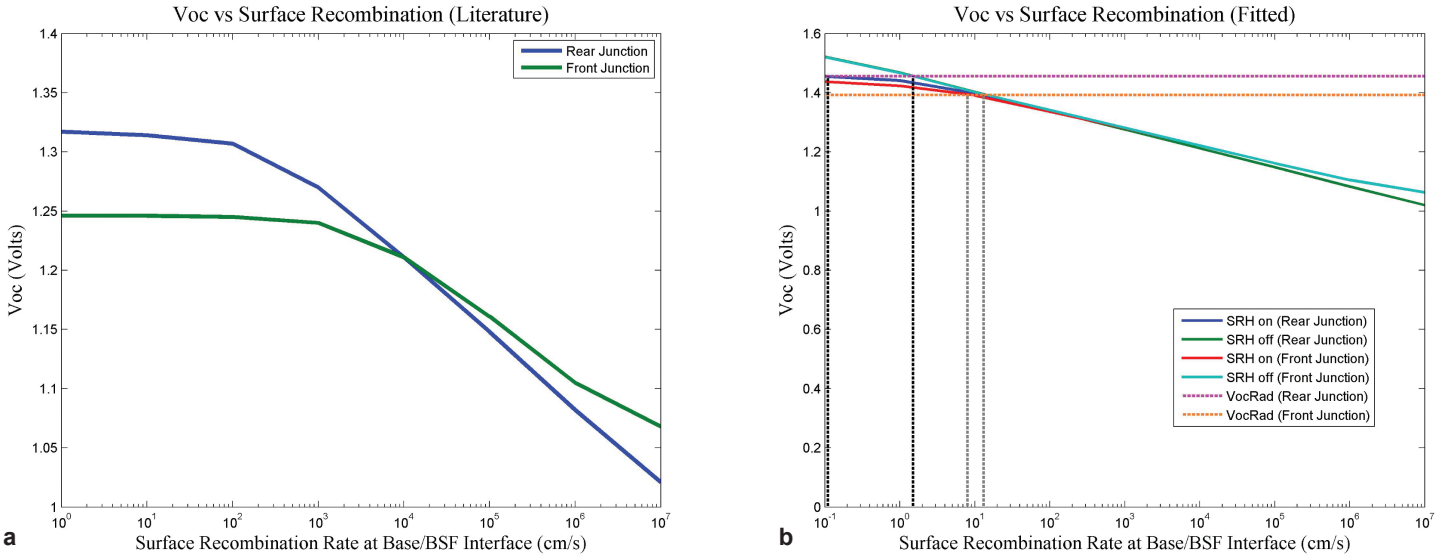


**Figure 12.** The simulated effects of varied surface recombination coefficients at the base/BSF interface. The black dashed lines in (b) indicate the possible range of surface recombination for the rear-junction structure, while the dashed gray lines indicate the range for the front-junction structure, assuming the fitted radiative B-coefficient is correct. Notice the effect of surface recombination can be seen at much lower surface recombination with the fitted values than with the literature values. Also, notice the relatively greater effect that surface recombination has on the rear-junction structure; this is particularly apparent in (a).

GaInP solar cell created by Geisz et al. (2013). The most conclusive answer thus far is that the bulk recombination is lowered in the rear-junction design that implements a junction with a small depletion width. This likely occurs because the large electric field collects carriers more quickly and because the lower doping density in the bulk region of the rear-junction structure results in fewer defects. Lower surface recombination may also play a key role.

The success of the rear-junction design would not be possible without the increased material quality that has recently become available to researchers. Increased material quality means fewer defects; fewer defects mean higher SRH lifetimes; and higher SRH lifetimes mean fewer losses in the bulk region, even if most of the generated carriers in the rear junction have to travel farther before they reach the junction. The fitted SRH lifetime of 70 µs may be unrealistically large, but even the literature value of 1 µs would have been unfeasible not very long ago.

Taking advantage of lower bulk SRH recombination rates was critical in this design, and it will be a focal point in designing and testing new types of solar cells in the future. One project we have considered is that of a "junctionless" solar cell: a cell that is essentially an intrinsic semiconductor with passivated surfaces. Such a cell would rely entirely on diffusion, rather than on the electric drift of the p-n junction, to collect carriers. It would see good lifetimes because an intrinsic semiconductor would not have as many defects as a doped semiconductor, and it would be extremely cheap and easy to manufacture. Intriguingly, as the base of the GaInP cell considered in this work becomes vanishingly small, the cell begins to resemble a junctionless device. While likely not what Geisz et al. (2013) had in mind when developing their rear-junction design, a junctionless solar cell is the sort of device that must be considered as the path to a future of renewable, sutainable energy continues to be forged by way of photovoltaic technology.

## ACKNOWLEDGMENTS

The author would like to thank Dr. Peter Bermel and Dr. Xufeng Wang for their input and support. Funding was provided through the Semiconductor Research Corporation Undergraduate Research Opportunities (SRC URO).

## REFERENCES

Bowden, S., & Honsberg, C. (2014). PVCDROM. Retrieved from http://pveducation.org/pvcdrom

Brown, M. R., Cobley, R. J., Teng, K. S., Rees, P., Wilks, S. P., Sobiesierski, A., . . . Blood, P. (2006). Modeling multiple quantum barrier effects and reduced electron leakage in red-emitting laser diodes. *Journal of Applied Physics*, *100*(8), 084509. http://dx.doi.org/10.1063/1.2362906

Gaubas, E., & Vanhellemont, J. (2007). Comparative study of carrier lifetime dependence on dopant concentration in silicon and germanium. *Journal of the Electrochemical Society*, *154*(3), H231–H238. http://dx.doi.org/10.1149/1.2429031

Geisz, J. F., Steiner, M. A., Garcia, I., Kurtz, S. R., & Friedman, D. J. (2013). Enhanced external radiative efficiency for 20.8% efficient single-junction GaInP solar cells. *Applied Physics Letters*, *103*(4), 041118. http://dx.doi.org/10.1063/1.4816837

Green, M. A., Emery, K., Hishikawa, Y., Warta, W., & Dunlop, E. D. (2015). Solar cell efficiency tables (Version 45). *Progress in Photovoltaics: Research and Applications*, *23*(1), 1–9. http://dx.doi.org/10.1002/pip.2573

Haas, A. W., Wilcox, J. R., Gray, J. L., & Schwartz, R. J. (2011). Design of a GaInP/GaAs tandem solar cell for maximum daily, monthly, and yearly energy output. *Journal of Photonics for Energy*, *1*(1), 018001–018001. http://dx.doi.org/10.1117/1.3633244

Ioffe Physico-Technical Institute. (2001). New semiconductor materials: Characteristics and properties. Retrieved from http://www.ioffe.ru/SVA/NSM/Semicond/GaInP/electric.html

Kayes, B. M., Nie, H., Twist, R., Spruytte, S. G., Reinhardt, F., Kizilyalli, I. C., & Higashi, G. S. (2011, June). 27.6% conversion efficiency, a new record for single-junction solar cells under 1 sun illumination. In *Photovoltaic Specialists Conference (PVSC), 2011 37th IEEE* (pp. 000004–000008). IEEE.

King, R. R., Fetzer, C. M., Colter, P. C., Edmondson, K. M., Law, D. C., Stavrides, A. P., . . . Karam, N. H. (2003, May). Lattice-matched and metamorphic GaInP/GaInAs/Ge concentrator solar cells. In *Proceedings of 3rd World Conference on Photovoltaic Energy Conversion* (Vol. 1, pp. 622–625). IEEE.

Kurtz, S. R., Myers, D., & Olson, J. M. (1997, September). Projected performance of three-and four-junction devices using GaAs and GaInP. In *Conference Record IEEE Photovoltaic Specialists Conference* (Vol. 26, pp. 875–878). IEEE. http://dx.doi.org/10.1109/pvsc.1997.654226

Lush, G., & Lundstrom, M. (1991). Thin film approaches for high-efficiency III–V cells. *Solar cells*, *30*(1), 337–344. http://dx.doi.org/10.1016/0379-6787(91)90066-X

Shockley, W., & Queisser, H. J. (1961). Detailed balance limit of efficiency of p-n junction solar cells. *Journal of Applied Physics*, *32*(3), 510–519. http://dx.doi.org/10.1063/1.1736034

Zhang, Y. G., & Gu, Y. (2012). Al(Ga)InP-GaAs photodiodes tailored for specific wavelength range. In I. Yun (Ed.), *Photodiodes—From Fundamentals to Applications*. INTECH Open Access Publisher. http://dx.doi.org/10.5772/50404